PAPER REF: To be completed by the Editors

APPLICATION OF INFRARED THERMOGRAPHY TO THE DAMAGE IDENTIFICATION IN A COLD-SPRAYED COPPER COATING

Chiara Colombo[1(*)], Antonio Salerno[2], Asghar Heydari Astaraee[1], Sara Bagherifard[1]

[1]Department of Mechanical Engineering, Politecnico di Milano, Milan, Italy
[2]Department of Energy, Politecnico di Milano, Milan, Italy
[(*)]*Email:* chiara.colombo@polimi.it

ABSTRACT

The work focuses on a cold-sprayed copper coating generated on a PEEK substrate. The main methodology to analyse pre-existing defects and damages generated during loading is infrared thermography. Pulsed thermography, used as a non-destructive technique, allows identifying defects generated due to the manufacturing process in terms of position and size (0.04-1.04 mm^2); they were detected also by SEM images, underlying decohesive cracking and delamination. Besides, thermographic monitoring during the static tensile tests allows estimating the damage initiation stress σ_D equal to 17.4 MPa for the coating. Eventually, from the mechanical output and thermal monitoring, it was possible to estimate E_{Cu} = 43930 MPa and UTS_{Cu}=78.6 MPa. Hence, these thermographic applications are efficient tools to characterize cold-sprayed coatings, understand their mechanical performances and support the design of functionalized components.

Keywords: Thermography, damage detection, cold spray.

INTRODUCTION

Cold Spray (CS) is a coating deposition technique exploiting the kinetic energy of accelerated particles to generate severe plastic deformation, primarily used for metal-on-metal and metal-on-plastic coatings (Moridi *et al.*, 2014). This last application, known as polymer metallization, improves the thermal, electrical, wear and erosion properties of polymers and composites with polymeric matrix (Parmar *et al.*, 2022). Cold spray application to polymers is a quite recent field of research and requires a selection of the most suitable experimental techniques to investigate inherent defects induced during manufacturing or caused by mechanical loading. While as-fabricated micro-pores and inter-particle boundaries are common in CS deposits, caused by insufficient particle plastic deformation and poor inter-particle bonding during deposition, CS copper coatings seldom experience micro-pores, thanks to the excellent ductility and low strength-to-density ratio of copper. Thus, for copper, the dominant defect that reduces the mechanical properties is the inter-particle boundaries (Raoelison *et al.*, 2016; Yin *et al.*, 2018). This type of defect has a negative effect on the mechanical properties, and it is, therefore, useful to apply thermal treatments such as annealing, in order to reduce them. In the case of surface metallization of polymers or composites, such thermal treatments are not applicable due to the low melting temperature of the substrate. Hence, it is essential to manufacture cold spray coating with optimized spraying parameters.

Nevertheless, defects are inevitable and always statistically present in the as-built coating and Non-Destructive Techniques (NDT) play a crucial role in the investigation and understanding

of the mechanical behavior of the coating when a load is applied. Infrared (IR) thermography could be an interesting tool for these purposes (Maldague, 1993; Heydari Astaraee *et al.*, 2021).

This work aims to detect the presence of defects and damages in a copper coating deposited on a polyether ether ketone (PEEK) substrate. Successful metallization of PEEK substrate using micron-sized copper powders has been reported by literature works (Gillet *et al.*, 2019; Heydari Astaraee, Colombo and Bagherifard, 2021, 2022; Raoelison, Lalu Koithara and Costil, 2021), mainly to enhance electrical and thermal properties of polymeric composites for aerospace applications. More in general, however, even low loads can induce crack propagation, lack of adhesion or concurrent mechanisms that can lead to premature failures of the coatings and loss of functionalization for the substrate.

This work considers pulsed thermography for the defects' detection in terms of location and size. Furthermore, the work presents another IR application of thermography to monitor the thermal response of the coating during the application of static loads. According to some experiments (Clienti *et al.*, 2010; Vergani, Colombo and Libonati, 2014), the variation in surface temperature can evidence irreversible damages progressively generated. It was suggested that the stress σ_D at the end of the thermoelastic stage corresponds to damage initiation. This stress could be very useful to design polymeric or composite components with the CS coating.

MATERIALS AND METHODS

Tensile specimens are cut from flat panels of unreinforced PEEK (RS Components S.r.l., Sesto San Giovanni, Milan, IT) from ISO 527-2 standard. Three specimens are cold sprayed with Cu particles. The cold spray system is the high-pressure Impact Innovations 5/8 (Impact Innovations GmbH, Rattenkirchen, Germany). The process and gas carrier is nitrogen. Spraying parameters are the following: average particle size 22.78 µm (Safina a.s, Vestec, CZ), pressure 4 MPa, temperature 300°C, nozzle transverse speed 30 mm/s, feed rate 25 g/min, standoff distance 40 mm, and hatching distance 2 mm. The hatching direction is perpendicular to the loading axis of the specimens, and the coating layer is generated in a single step. These parameters were selected after some experimental trials, optimized for this combination of substrate and powders. The thickness of the PEEK is 5.4 mm, and the thickness of the Cu coating is 0.45 mm (see Fig. 1a). The specimens are sprayed on both faces, to avoid bending during the uniaxial static tests, e.g., obtaining a symmetric specimen with respect to the load axis.

Pulsed IR thermography was selected to investigate the surface of the coated specimens. This is a screening tool to understand the presence of pre-existing defects due to the manufacturing, before performing the tensile tests. An IR thermal camera (X6900sc model, by Teledyne FLIR LLC, Wilsonville, Oregon, USA) with a cooled InSb sensor having a thermal sensitivity/NETD lower than 20 mK is used to monitor the surface temperature variation as a function of the time. The acquisition starts before the thermal pulse is generated with a halogen lamp (Model Style RX 1200, by Elinchrom, Renens, CH). Fig. 1b shows a schematic representation of the experimental setup. The 25 mm lenses are mounted, placing the thermal camera perpendicular to the specimen surface, at a distance of about 170 mm. The thermal matrices are stored with a spatial resolution of 0.2 mm/pixel and an acquisition frequency of 1920 Hz. Data storage and analysis are performed with the software ResearchIR Max (version 4.40.11, by Teledyne FLIR LLC, Wilsonville, Oregon, USA). Raw thermal data are processed with the normalizing function proposed in (Heydari Astaraee *et al.*, 2021):

$$\hat{T}(i,j,t) = \frac{T(i,j,t) - T(i,j,t=0)}{T(i,j,t=1) - T(i,j,t=0)} \quad (1)$$

where *i* and *j* are the variables spanning row and columns of the raw thermal matrix, *t* is the time and *T* is the temperature. *T(i,j,t=0)* is the image before the flash, *T(i,j,t=1)* is the image immediately after the flash (i.e., the peak recorded temperature), and *T(i,j,t)* is the image at the generic time *t*. This normalization procedure is necessary to avoid reflection of external sources, non-uniform heating of the source a non-uniform thermal emissivity that can affect the IR thermal signal.

Together with the specimens, also some coupons were sprayed to check the presence of defects through the thickness generated during the CS manufacturing, with a destructive procedure to compare with the non-destructive thermographic results. These coupons have a size of 50x50 mm^2 and are sprayed on one single side with the same CS parameters as the specimens. After carefully sectioning the sprayed coupons, images of the cross-section are collected and analyzed with a Scanning Electron Microscope (SEM, model EVO 50XVP by Zeiss, Oberkochen, DE).

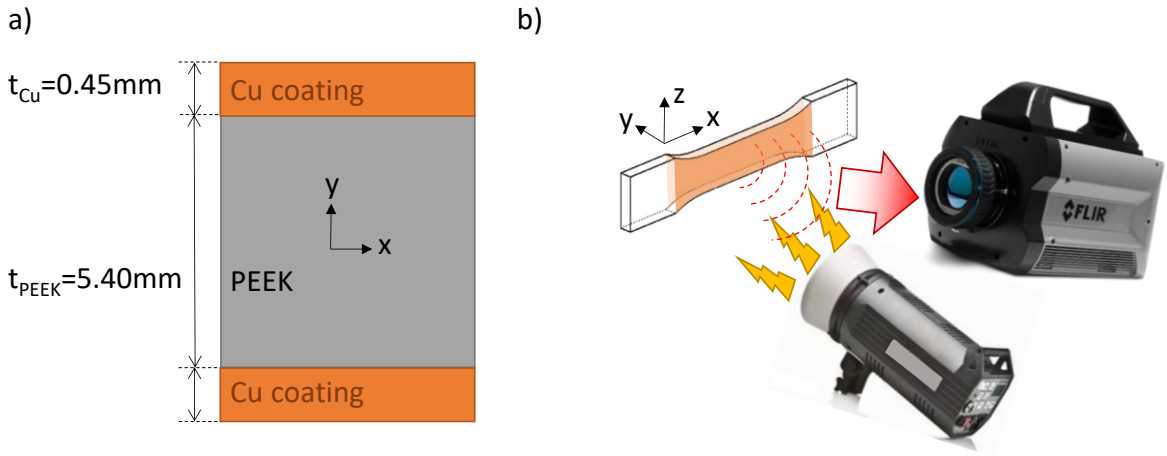

Fig. 1 – a) Schematization of the through-thickness section of the specimen;
b) experimental setup for the tests of pulsed thermography.

Static tests are performed following the ISO 527-2:2012 standard on three specimens made of unreinforced PEEK and on the three cold-sprayed ones. During the static tests at 2 mm/min, the thermal camera records the temperature changes on the surface of the specimen with the setup shown in Fig. 2a. The load cell output is acquired as an input for the IR camera during the mechanical loading. An extensometer (Model 634.12F-54, by MTS Systems, Eden Prairie, Minnesota, USA), laterally mounted, recorded the strains (see Fig. 2b). Thus, the outputs of the tests are: 1) the applied load and the corresponding stress, 2) the strain in the central portion of the specimen, 3) the surface thermal maps that allow analyzing the temperature variation with respect to the beginning of the test. The temperature is averaged over the central portion of the specimen, and then plotted as a function of the test time to identify the damage initiation as the stress at the end of the thermoelastic stage. This stress σ_D is estimated from a linear fitting of the temperature variation vs time, selecting the thermal data with a statistical coefficient of determination R^2 higher than 99%.

Fig. 2c shows some failed specimens after the tensile test.

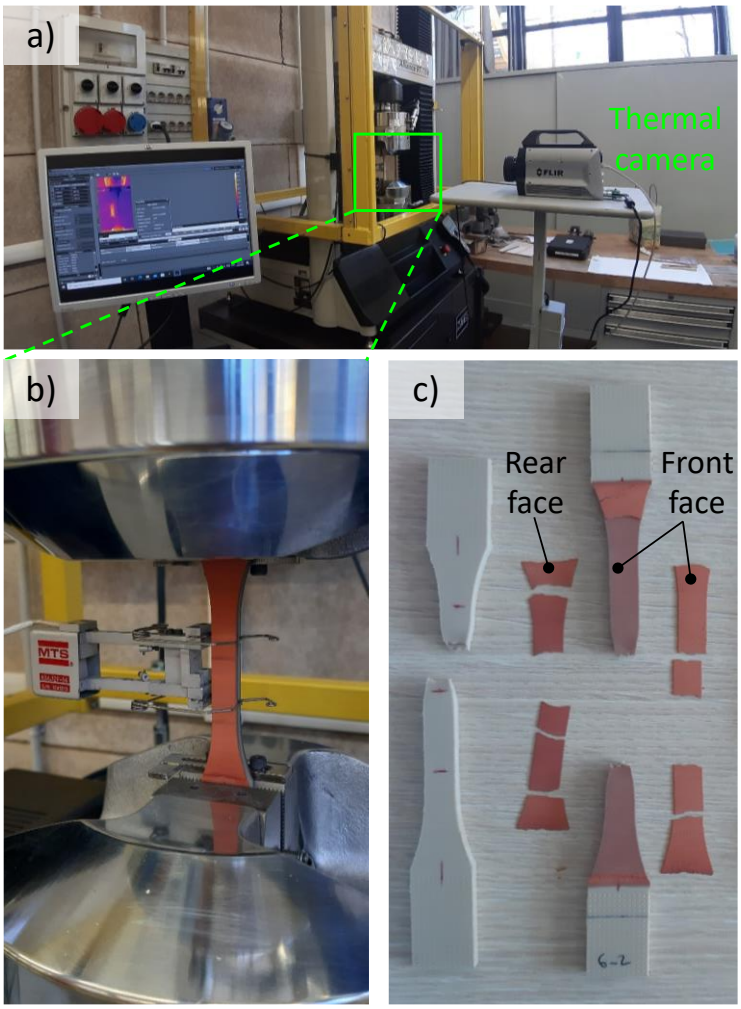

Fig. 2 – a) Experimental setup for the static test with thermographic monitoring; b) detail of the coated specimen; c) failed uncoated and coated specimens after the test.

RESULTS

Identification of pre-existing defects

Fig. 3a shows the normalized thermal map of a coated specimen, where some anomalies are identified. Indeed, some small regions, magnified in Fig. 3b, experience a lower decrease in the normalized temperature as a function of the time with respect to the rest of the coated specimen, e.g. supposed to be defect-free and considered as a reference region. This thermal trend is typical of existing defects, e.g. (Ibarra-Castanedo and Maldague, 2004). Although these defects are very small, the pulsed thermography allows identifying their location and approximate size in the plane projected on the coated surface, ranging from 1 pixel (0.04 mm^2) for region 2 to a more complex C-shape of 26 pixels (1.04 mm^2) for region 1, see Fig. 3b. Fig. 3c shows the thermal decays in these regions containing defects; the curves are higher than the reference region of the coating, but lower than the uncoated PEEK.

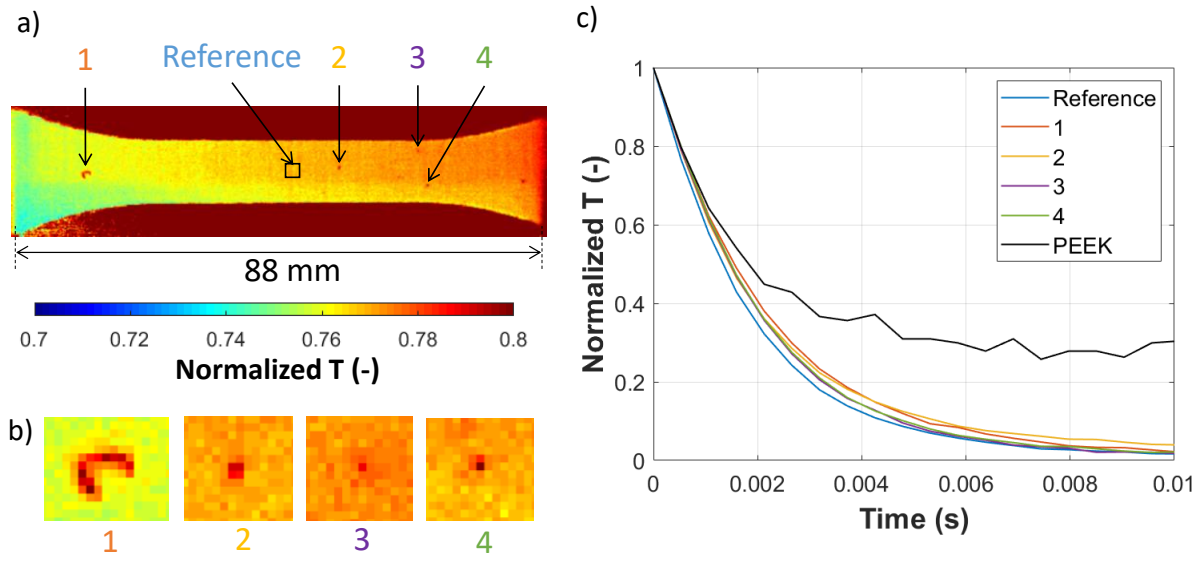

Fig. 3 – a) Normalized thermal map of a coated specimen during the pulsed thermographic test; b) magnification of some thermal anomalies; c) trend of the normalized temperature as a function of the time for different regions of the specimen.

In order to better understand the type of these defects, the SEM investigation is also performed, obtaining the images of Fig. 4. By this destructive technique, it is possible to state that the porosity of the coating is very limited, thanks to the ductility of the copper powders and the proper CS parameter selection. However, a few cracks are detected, such as the one shown in this image. This crack lays through the coating along the impact direction of the particles (y-axis), but also branches at the interface between the PEEK substrate and the Cu coating (x-axis). The crack size is about 100 µm in the y direction, but it is more complex to estimate the root extension along the x-axis, e.g., at the interface with the substrate.

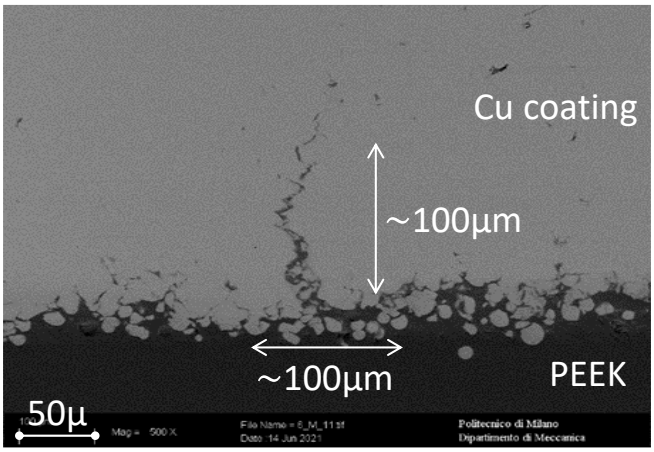

Fig. 4 – SEM image of a crack located in the coating but also branching at the PEEK-Cu interface.

Thermal trends during static tests

Fig. 5 shows the experimental curves in terms of stress vs strain (Fig. 5a and its magnification in Fig. 5b) and of stress and surface temperature variation vs time (Fig. 5c and d). These last ones are used to estimate the damage stress σ_D, at the end of the thermoelastic stage. Table 1 summarizes the corresponding mechanical properties and σ_D, estimated from the thermo-mechanical curves.

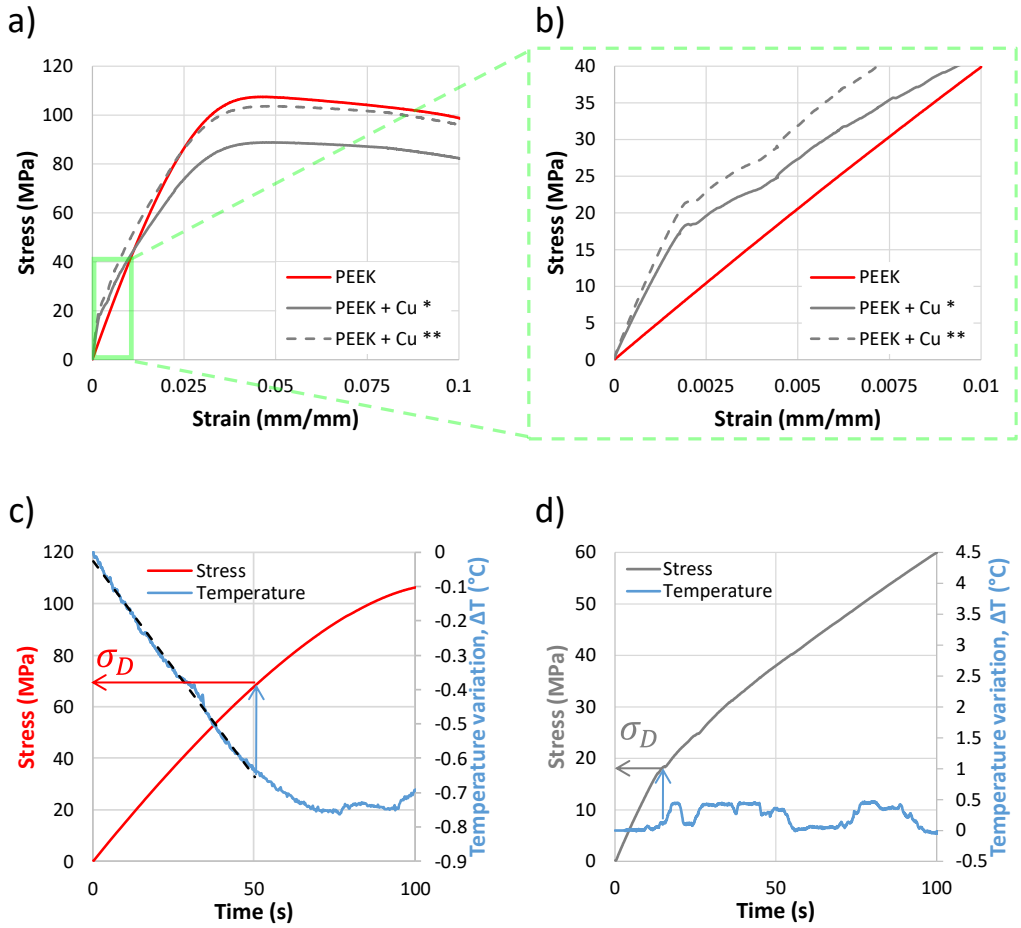

Fig. 5 – Mechanical and thermal results from the static tests. a) Stress vs strain curve and b) its magnification up to 0.01 mm/mm for the uncoated and the coated specimens (*: The stress is obtained by dividing the load by the initial dimension of the cross-section, e.g., PEEK and coating; **: The stress is obtained by dividing the load by the cross-section of the only PEEK). Stress and temperature curves as a function of time for c) uncoated and d) coated specimens, with the identification of the thermal damage stress σ_D.

Table 1: Summary of the results from the experimental static tensile tests (*: The stress is obtained by dividing the load by the initial dimension of the cross-section, e.g., PEEK and coating; **: The stress is obtained dividing the load by the cross-section of the only PEEK).

	E (MPa)	YS (MPa)	UTS (MPa)	ε_f (%)	σ_D (MPa)
PEEK	4052±136	73.3±5.9	108.3±2.1	19±13	63.1±9.5
Cu-coated PEEK	7546±83*	37.9±1.5**	103.0±1.5**	24±19	17.4±2.0*

DISCUSSION

The results from the pulsed thermographic tests of Fig. 3 evidence the presence of some defects in the coating generated during the manufacturing. This technique is fast and straightforward but has also some limitations. Indeed, it is worth mentioning that it does not allow for the identification of the specific damage that could be a decohesive crack in the coating, delamination at the interface with the substrate, voids, etc. Indeed, the thermal anomaly is the defect area projected on the surface. Hence, another known limitation of this technique is the difficulty to identify cracks exactly perpendicular to the scanned surface (Netzelmann and Walle, 2008), that actually can be present in the scanned specimens as from the SEM image of

Fig. 4. From this image we can hypothesize that the observed thermal anomalies evidence the size where a lack of adhesion occurred between the PEEK and the coating, e.g., the delamination in the x-z plane, without an effective detection of the crack extent along y, that is the direction of the particles' velocity. Indeed, cracks perpendicular to the surface to be inspected can become thermally active and detectable with other thermographic inspections, for instance based on the ultrasonic excitation (Rantala *et al.*, 1996; Salerno *et al.*, 1997).

When coated specimens or components are loaded, both the substrate and the coating itself are loaded. This means that pre-existing cracks can propagate and limit the functionalization of the substrate, e.g., if the coating starts cracking, the component could lose the electrical conductivity, or if it starts delaminating and detaching, the component could lose wear resistance. For this reason, it is interesting to monitor the mechanical and thermal behavior of the coating during the tensile test, to detect the damage initiation in terms of applied stress, namely the damage stress σ_D.

Before discussing the results of the coated specimens, it is worth analyzing the thermo-mechanical behavior of the uncoated PEEK specimens. All the PEEK mechanical properties of Table 1 agree with the manufacturer's data sheet (*RS Components S.r.l.*, 2023) and with other literature works collected in a database (*MatWeb, LLC.*, 2023). Fig. 5c shows in detail the end of the thermoelastic stage and the identification of the σ_D for a PEEK specimen. For the pure PEEK, $\sigma_{D,PEEK}$=63.1MPa is about 10 MPa lower than yielding (see Table 1), e.g., the thermographic technique identifies some irreversible micro-damages into the polymer before the global mechanical deviation from linearity occurs. At the beginning of the load application, due to the thermoelastic effect, the materials typically cool down with a linear trend. Then, when some damage occurs, the temperature deviates from linearity, progressively reaches a minimum, and subsequently the specimen begins warming up. This underlines the irreversible nature of the damage. It was proposed in the literature that, for plastic materials, the stress σ_D at the end of the thermoelastic linear stage corresponds to the damage initiation, and it is an estimation of the fatigue strength (Clienti *et al.*, 2010).

Moving to the coated specimens, static tests revealed a premature failure of the copper, due to the different stiffness with respect to the polymer and to poor adhesion between the substrate and coating. The coating cracked perpendicularly to the load direction and detached from the substrate before the end of the test. The visual inspection of the failed specimens at the end of the test (Fig. 2c) evidences that only a few particles remained attached to the PEEK, suggesting that not only a cohesive but also an adhesive failure occurs. These failures in the Copper occur at the early stage of the static test, below the damage stress of the PEEK substrate, as suggested from the stress-strain curve of Fig. 5a,b. The Cu coating is fully adherent to the polymer up to about 17 MPa nominal stress, experiencing a linear stress-strain curve as in the solid grey curve of Fig. 5b. Hence, the elastic modulus E and the damage stress σ_D of the coated specimen given in Table 1 are calculated considering the nominal cross-section, sum of the PEEK and copper layers. Indeed, σ_D identifies the beginning of the damage, as estimated from the thermographic measurement, showing a sudden temperature increase. Beyond this stress level, the coating progressively damages, starts cracking and loses its adhesion with the substrate before the macroscopic variation from the linear stress-strain behavior occurs. Therefore, the stress higher than σ_D should be progressively calculated from the net cross-section, which eventually becomes equal to that one of the only polymer. The yield stress (YS) and ultimate strength (UTS) of these specimens are calculated considering the cross-section of the only polymer, as in the dashed grey curve of Fig. 5b and in Table 1.

From the thermal monitoring of the static test, the Cu-sprayed PEEK experiences the unexpected behavior of Fig. 5d. The cooling phase does not occur, and the specimen has almost a flat thermal trend as a function of the time and, hence, of the applied displacement. This can be explained with the high thermal diffusivity ($\alpha = \frac{\kappa}{\rho c}$) and effusivity (e=$\sqrt{\kappa \rho c}$ with κ = thermal conductivity, ρ = mass density and c = specific heat) of the copper coating Therefore, the elastic stage is not present and the damage occurs almost immediately with the load application. The sudden increases in the surface temperature, followed by rapid cooling at the initial temperature, may be due to the accumulation of damages during the loading of the sample leading to local fractures of the coating. It is likely that some cracking is happening, but due to the high thermal conductivity of the copper and to its low thickness, the heat is soon dissipated. The first thermal jump can identify the $\sigma_{D,PEEK+Cu}$=17.4 MPa, which corresponds to the damage strain ε_D = 0.179% common to PEEK and Cu coating, e.g., the failure is extremely brittle because the thermal and mechanical deviations from linearity are coincident. This result suggests that the coated layer is highly brittle; indeed, it is well known that copper is a very ductile material, but the cold-sprayed layer is in the as-built condition.

Given these mechanical and thermal results, it is possible to add further points to this discussion. Indeed, the results of the experimental static tests allow for estimating some mechanical properties of the Cu coating. Supposing initial full adhesion between the PEEK and the sprayed copper during the linear stage of the stress-strain curve, we can use the rule of thumbs to estimate E_{Cu}:

$$\sigma_{D,PEEK+Cu} = \sigma_{PEEK} \cdot \frac{t_{PEEK}}{t_{tot}} + \sigma_{Cu} \cdot \frac{t_{Cu}}{t_{tot}} = E_{PEEK} \cdot \varepsilon_D \cdot \frac{t_{PEEK}}{t_{tot}} + E_{Cu} \cdot \varepsilon_D \cdot \frac{t_{Cu}}{t_{tot}} \quad (2)$$

where t_{tot} is the total thickness of the specimen, sum of t_{PEEK} = 5.4 mm and t_{Cu} = 0.9mm, which is the total Cu thickness of the two layers. Knowing E_{PEEK} from Table 1, the elastic modulus of the copper layer is:

$$E_{Cu} = \frac{\sigma_{D,PEEK+Cu}}{\varepsilon_D} \cdot \frac{t_{tot}}{t_{Cu}} - E_{PEEK} \cdot \frac{t_{PEEK}}{t_{Cu}} \quad (3)$$

Eq. 3 gives the estimation E_{Cu} = 43930 MPa for the cold-sprayed copper layers.

Besides, it is possible to give a rough estimation of the cohesive strength of the sprayed coatings, under the hypothesis that they experience a fully brittle behavior, e.g., linear elastic up to failure. Therefore, the ultimate tensile strength of the copper UTS_{Cu} is simply obtained as:

$$UTS_{Cu} = E_{CU} \cdot \varepsilon_D \quad (4)$$

This equation leads to the estimation UTS_{Cu}=78.6 MPa for the specimen of Fig. 5b. This value of cohesive strength is similar to another literature work of mechanical characterization of a copper cold sprayed layer obtained with similar manufacturing parameters (Raoelison, Lalu Koithara and Costil, 2021), as well as to the study (Gärtner *et al.*, 2006) on self-standing cold-sprayed Cu specimens.

However, as previously mentioned, from the failed specimens of Fig. 2c it is evident that another failure mode also occurs due to the low adhesion between the coating and the substrate. It is difficult to estimate the adhesive strength from the mechanical and thermal information collected during this static tensile test. Indeed, also the thermal monitoring could not evidence any local heating or anomalies during the early stage of the load application. It is not clear if the coating's cracking occurred before the delamination, e.g., if the failure occurs due to decohesion or lack of adhesion, or vice versa.

Future works to clarify the effective failure mode of the coating will require experimental adhesive tests to estimate the adhesion strength, which could be very low, e.g., in the order of maximum 10 MPa (Raoelison, Lalu Koithara and Costil, 2021). Once the cohesive and adhesive strengths are known, a numerical model of the coated specimen, including pre-existent defects similar to the one in Fig. 4, could shed light on the actual failure mechanism of the coating.

CONCLUSIONS

An experimental campaign of mechanical characterization was carried out on PEEK specimens coated with a copper deposit through the cold spray technique. IR thermography has been proved as a twofold tool, suitable for:

- the identification of defects generated during the manufacturing in terms of position and size. Pulsed thermography evidenced pre-existing defects from 0.04 mm^2 to 1.04 mm^2 in the coated specimens; this size is the defect's projection on the surface. The presence of as-built defects was supported also by SEM images, which evidenced both decohesive cracking and delamination at the interface with the substrate;
- the damage monitoring during static tensile tests, allowing for the estimation of the damage initiation stress σ_D. The thermographic damage stress is 63.1 MPa for the uncoated PEEK, but it decreases to 17.4 MPa for the coating, meaning that the copper starts damaging at the early stage of load application. Crossing the information from the mechanical stress-strain curve and the thermal maps collected during the test, it was possible to estimate the elastic modulus and the ultimate tensile strength of the cold-sprayed copper, respectively equal to E_{Cu} = 43930 MPa and UTS_{Cu}=78.6 MPa. These values are useful for the design of components with cold spray coatings.

AKNOWLEDGEMENTS

The research leading to these results has received funding from the Italian Ministry of University (MUR) under the call "Progetti di Ricerca di Rilevante Interesse Nazionale - PRIN", grant number 2017N4422T (COSMEC).

REFERENCES

[1] Clienti, C. *et al.* (2010) 'A first approach to the analysis of fatigue parameters by thermal variations in static tests on plastics', *Engineering Fracture Mechanics*, 77(11), pp. 2158–2167. doi: 10.1016/j.engfracmech.2010.04.028.
[2] Gärtner, F. *et al.* (2006) 'Mechanical properties of cold-sprayed and thermally sprayed copper coatings', *Surface and Coatings Technology*, 200(24), pp. 6770–6782. doi: 10.1016/j.surfcoat.2005.10.007.
[3] Gillet, V. *et al.* (2019) 'Development of low pressure cold sprayed copper coatings on carbon fiber reinforced polymer (CFRP)', *Surface and Coatings Technology*, 364, pp. 306–316. doi: 10.1016/j.surfcoat.2019.01.011.
[4] Heydari Astaraee, A. *et al.* (2021) 'Thermographic analysis of composite metallization through cold spray', *Metals*, 11(11). doi: 10.3390/met11111860.
[5] Heydari Astaraee, A., Colombo, C. and Bagherifard, S. (2021) 'Numerical Modeling of Bond Formation in Polymer Surface Metallization Using Cold Spray', *Journal of Thermal Spray Technology*. doi: 10.1007/s11666-021-01224-9.
[6] Heydari Astaraee, A., Colombo, C. and Bagherifard, S. (2022) 'Insights on metallic particle

bonding to thermoplastic polymeric substrates during cold spray', *Scientific Reports*, 12(1). doi: 10.1038/s41598-022-22200-5.
[7] Ibarra-Castanedo, C. and Maldague, X. (2004) 'Pulsed phase thermography reviewed', *Quantitative InfraRed Thermography Journal*, 1(1), pp. 47–70. doi: 10.3166/qirt.1.47-70.
[8] Maldague, X. P. V. (1993) *Nondestructive Evaluation of Materials by Infrared Thermography*, *Nondestructive Evaluation of Materials by Infrared Thermography*. London, UK: Springer Verlag. doi: 10.1007/978-1-4471-1995-1.
[9] *MatWeb, LLC.* (2023). Available at: https://www.matweb.com/ (Accessed: 3 November 2022).
[10] Moridi, A. *et al.* (2014) 'Cold spray coating: Review of material systems and future perspectives', *Surface Engineering*, 30(6), pp. 369–395. doi: 10.1179/1743294414Y.0000000270.
[11] Netzelmann, U. and Walle, G. (2008) 'Induction thermography as a tool for reliable detection of surface defects in forged components', in *17th WCorld Conference on NDT, Shanghai, China*, p. 8.
[12] Parmar, H. *et al.* (2022) 'Metallisation of polymers and polymer matrix composites by cold spray: state of the art and research perspectives', *International Materials Reviews*, 67(4), pp. 385–409. doi: 10.1080/09506608.2021.1954805.
[13] Rantala, J. *et al.* (1996) 'Lock-in thermography with mechanical loss angle heating at ultrasonic frequencies'. doi: 10.21611/qirt.1996.064.
[14] Raoelison, R. N. *et al.* (2016) 'Low pressure cold spraying under 6 bar pressure deposition: Exploration of high deposition efficiency solutions using a mathematical modelling', *Surface and Coatings Technology*, 302, pp. 47–55. doi: 10.1016/j.surfcoat.2016.05.068.
[15] Raoelison, R. N., Lalu Koithara, L. and Costil, S. (2021) 'Cold spray coating of PEEK surface by copper deposition: Interfacial adhesion at high deposition efficiency and bonding strength', *CIRP Journal of Manufacturing Science and Technology*, 35, pp. 63–68. doi: 10.1016/j.cirpj.2021.05.008.
[16] *RS Components S.r.l.* (2023). Available at: https://www.rs-online.com/ (Accessed: 21 February 2023).
[17] Salerno, A. *et al.* (1997) 'Thermographic Inspection with Ultrasonic Excitation', *Review of Progress in Quantitative Nondestructive Evaluation*, pp. 345–352. doi: 10.1007/978-1-4615-5947-4_45.
[18] Vergani, L., Colombo, C. and Libonati, F. (2014) 'A review of thermographic techniques for damage investigation in composites', *Frattura ed Integrita Strutturale*, 8(27), pp. 1–12. doi: 10.3221/IGF-ESIS.27.01.
[19] Yin, S. *et al.* (2018) 'Cold spray additive manufacturing and repair: Fundamentals and applications', *Additive Manufacturing*, 21, pp. 628–650. doi: 10.1016/j.addma.2018.04.017.